Deep learning based reduced order modeling of seismogram-type acceleration time series model: Part - II

Saumik Dana[1*] and Karthik Reddy[2]

[1*]University of Southern California, Los Angeles, CA, USA.
[2]North Carolina State University, Raleigh, NC, USA.

*Corresponding author(s). E-mail(s): saumik@utexas.edu;
Contributing authors: klyatha@ncsu.edu;

Abstract

The Bayesian inference framework with the obvious invocation of Markov Chain Monte Carlo is computationally infeasible if the forward model is heavy. The reason is that the inference framework requires a huge number of forward simulation passes to arrive at robust estimates of the model parameter(s). In lieu of that, a reduced order model becomes critical. The LSTM based encoder decoder framework offers promise in that realm. The encoder effectively compresses all the solution information in dominant eigenmodes, and the decoder reconstructs the solution from those eigenmodes.

Keywords: Time series, LSTM, encoder, decoder, reduced order model

1 Introduction

The Bayesian framework for inference requires continuous evaluation of the forward model, which can get overbearingly expensive if the forward model is dense in computational physics. For that reason, it is incredibly important to construct reduced order model which will then be used to provide continuous evaluations within the Bayesian loop as shown in Fig. 1. With due regard to the mathematics behind singular value decompositions and principal component analysis for reduced order modeling, it can be difficult to operate on standalone

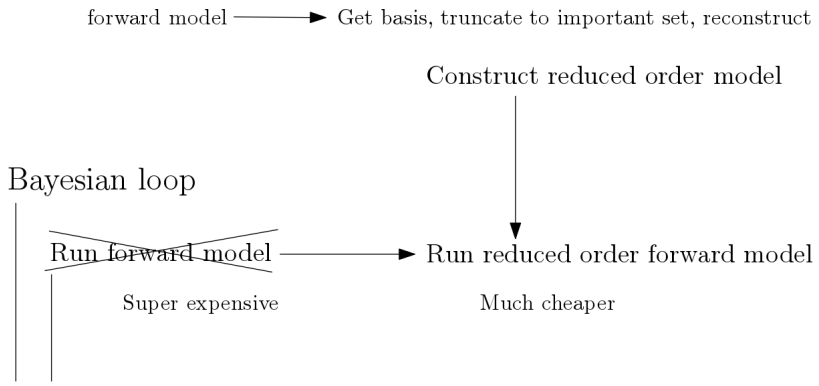

Fig. 1: The big picture

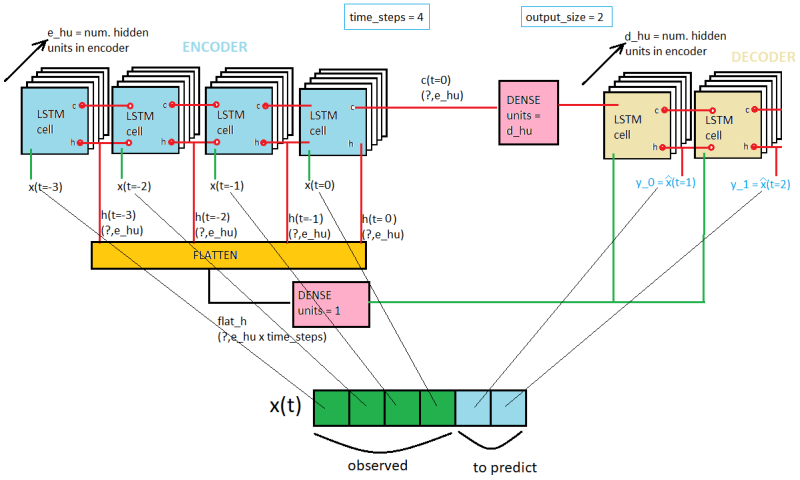

Fig. 2: LSTM encoder decoder

codes which do specific decompositions on specific time series based on the features to be captured. This is where the deep learning framework in either PyTorch or TensorFlow is incredibly useful, as they provide robust archetypal code bases to build reduced order models by throwing some intuition into the science of deep learning. Long short term memory (LSTM) [1] based encoder decoder architectures offer a convenient path towards reconstruction of time series solution, whether univariate or multivariate, and the framework in a nutshell is shown in Fig. 2. The encoder and decoder are themselves LSTM cells, single or multiple, and while the former compresses all the time series information into a latent vector, the latter decompresses the latent vector to reconstruct the time series. The LSTM cell itself is a little involved, as shown in Fig. 3. There are 3 gates: input, output and forget gate, and there are 2

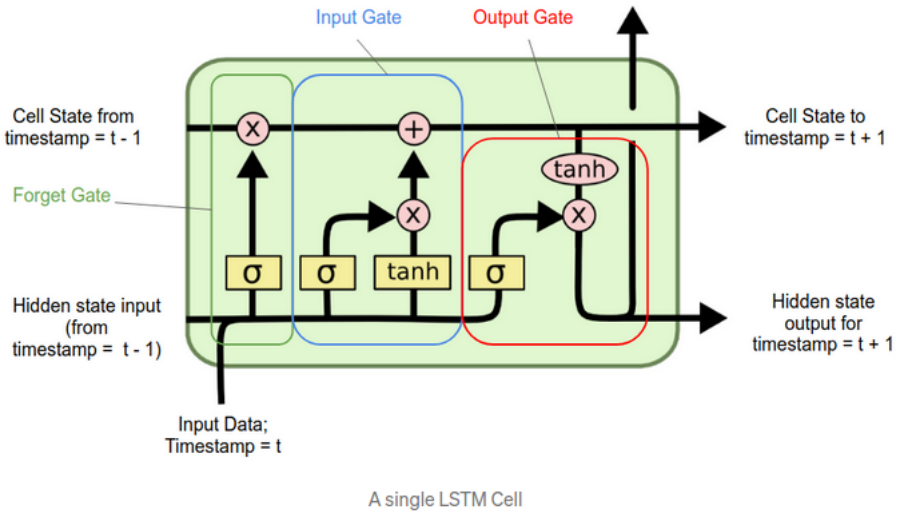

Fig. 3: Single LSTM cell

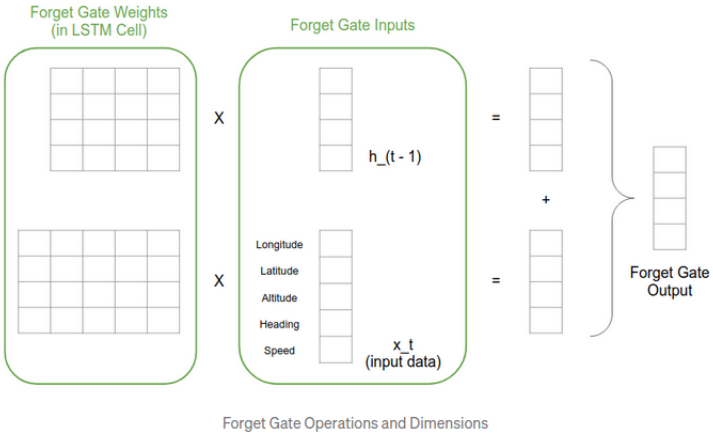

Fig. 4: Forget gate operations for hidden size of 4 and batch size of 1

states: cell state and hidden state. The operations within the vanilla LSTM are documented in literature, but there are some architectural parameters for the whole encoder decoder network like number of LSTM layers and size of hidden state which are important to understand. For example, a LSTM forget gate operations for a hidden size of 4 and batch size of 1 is shown in Fig. 4. On the other hand, a LSTM forget gate operation for a hidden size of 4 and batch size of 1 is shown in Fig. 5. We need to keep in mind that this entire effort

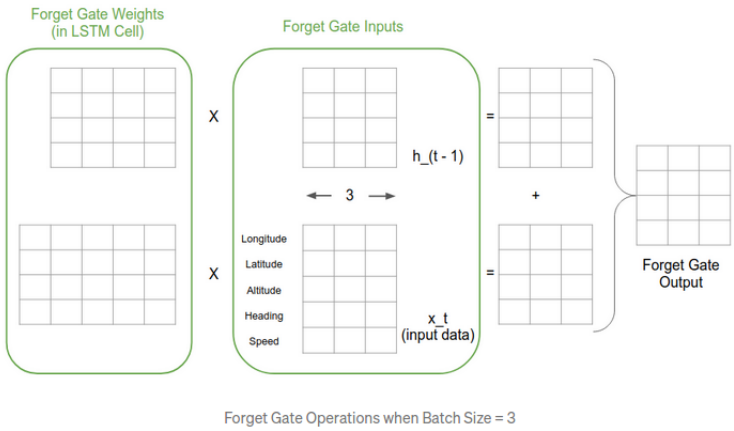

Fig. 5: Forget gate operations for hidden size of 4 and batch size of 3

is geared towards reduced order model reconstruction for Bayesian inference of parameters of a complicated forward model, but as always we start off with simpler forward models to provide the robustness of the concept before tacking the real challenge. The forward model, as explained in Appendix A, is that of the spring slider damper idealization of the rate and state model for fault friction for modeling seismic behavior in response to pressure and stress perturbations in the subsurface. The RSF model is a piece of the coupled flow and geomechanics [2–10] puzzle, and we are working on an idealization of the piece of the puzzle in itself. This goes to show the depth of this research endeavor, and it makes sense to take it one step at a time. In this study, we see how the size of the hidden state and the number of LSTM inside the encoder and decoder can impact the accuracy of the reconstruction.

2 Reconstruction results

The code was implemented in PyTorch, and run on a basic AMD Ryzen 3 3200U with Radeon Vega Mobile Gfx × 4 processor. We observe from Figs. 6 and 7 that the number of layers and size of hidden state when increased lead to better accuracy of the reconstructed solution. But it also evident that beyond a point, a better accuracy is more or less a heuristic measure, which points to the fact that the optimizer knowledge is equally important in this parlance. The batch size has been kept as 1 in all simulations, and we will pick up this particular batch size parameter in part-III of this series

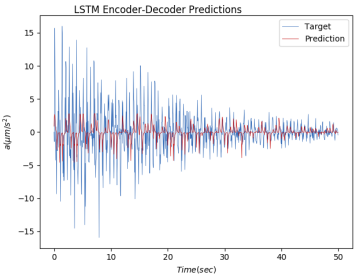

(a) Size of hidden state is 1

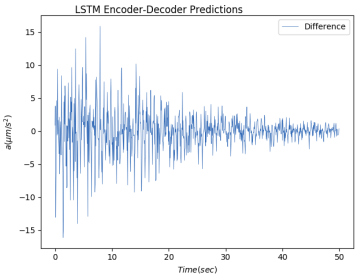

(b) Size of hidden state is 1

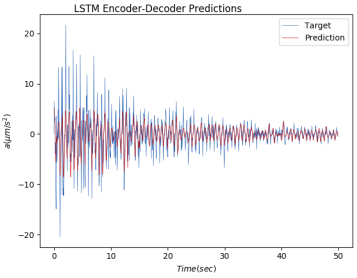

(c) Size of hidden state is 2

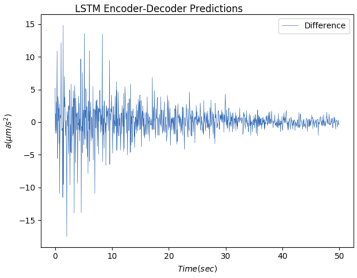

(d) Size of hidden state is 2

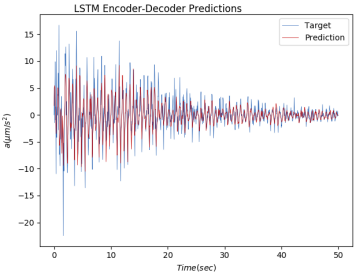

(e) Size of hidden state is 3

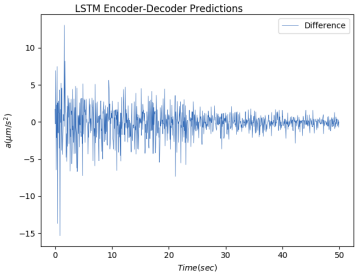

(f) Size of hidden state is 3

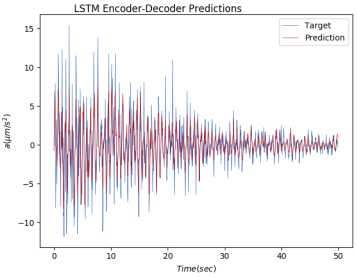

(g) Size of hidden state is 4

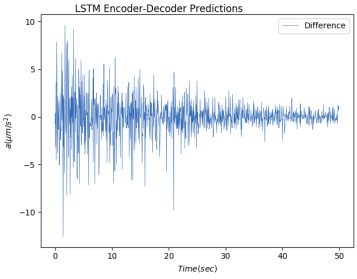

(h) Size of hidden state is 4

Fig. 6: Number of LSTM layers is 2

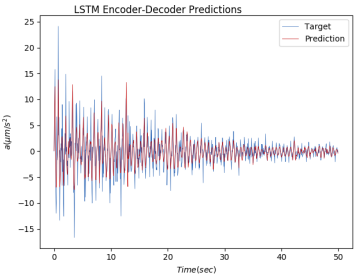

(a) Number of LSTM layers is 1

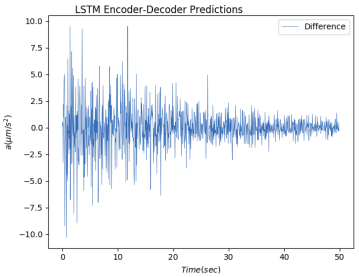

(b) Number of LSTM layers is 1

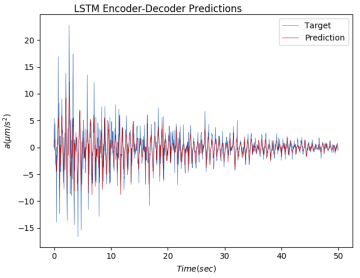

(c) Number of LSTM layers is 2

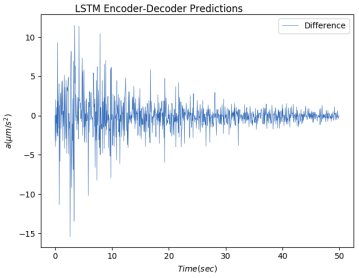

(d) Number of LSTM layers is 2

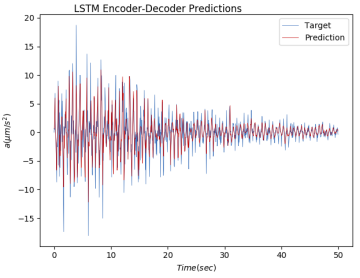

(e) Number of LSTM layers is 3

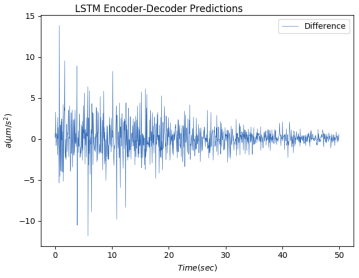

(f) Number of LSTM layers is 3

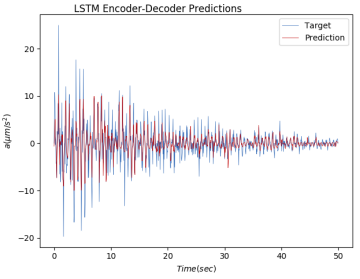

(g) Number of LSTM layers is 4

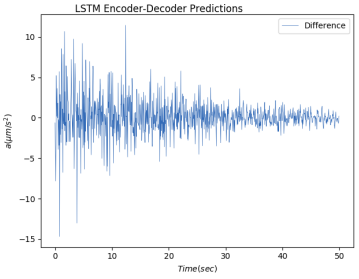

(h) Number of LSTM layers is 4

Fig. 7: Size of hidden state is 5

Appendix A Forward model details

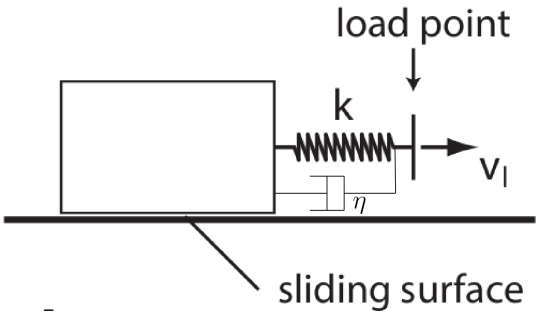

Fig. A1: Spring slider damper idealization of fault behavior

The quantification of fault slip is achieved using the rate- and state-friction (RSF) model for modeling earthquake cycles on faults [11–16], and given by

$$\mu = \mu_0 + A \ln\left(\frac{V}{V_0}\right) + B \ln\left(\frac{V_0 \theta}{d_c}\right), \quad \frac{d\theta}{dt} = 1 - \frac{\theta V}{d_c} \tag{A1}$$

where $V = |\frac{d\boldsymbol{d}}{dt}|$ is the slip rate magnitude, $a = \frac{dV}{dt}$ which we hypothesize is of the same order as recorded by seismograph, μ_0 is the steady-state friction coefficient at the reference slip rate V_0, A and B are empirical dimensionless constants, θ is the macroscopic variable characterizing state of the surface and d_c is a critical slip distance over which a fault loses or regains its frictional strength after a perturbation in the loading conditions [17]. As shown in Fig. A1, we model a fault by a slider spring system [18–20]. The friction coefficient of the block is given by

$$\mu = \frac{\tau}{\sigma} = \frac{\tau_l - k\delta - \eta V}{\sigma} \tag{A2}$$

where σ is the normal stress, τ the shear stress on the interface, τ_l is the remotely applied stress acting on the fault in the absence of slip, -$k\delta$ is the stress relaxation due to fault slip [21] and η is the radiation damping coefficient [22]. We consider the case of a constant stressing rate $\dot{\tau}_l = kV_l$ where V_l is the load point velocity. The stiffness is a function of the fault length l and elastic modulus E as $k \approx \frac{E}{l}$. With $k' = \frac{E}{l\sigma}$, we get

$$\dot{\mu} \approx k'(V_l - V) - k''\dot{V} \tag{A3}$$

where $k'' = \frac{\eta}{\sigma}$. Once the phenomenological form of $\dot{\mu}$ is known, we rewrite Eq. (A1) as

$$\begin{aligned} V &= V_0 \exp\left(\frac{1}{A}\left(\mu - \mu_0 - B\ln\left(\frac{V_0\theta}{d_c}\right)\right)\right), \\ \dot{\theta} &= 1 - \frac{\theta V}{d_c} \end{aligned} \tag{A4}$$

to get acceleration time series as $a \equiv \dot{V}$ as,

$$\begin{aligned} \dot{V} &= \frac{V}{A}\left(\dot{\mu} - \frac{B}{\theta}\dot{\theta}\right) \\ &= \frac{V_0 \exp\left(\frac{1}{A}\left(\mu - \mu_0 - B\ln\left(\frac{V_0\theta}{d_c}\right)\right)\right)}{A} \\ &* \left(k'\left(V_l - V_0 \exp\left(\frac{1}{A}\left(\mu - \mu_0 - B\ln\left(\frac{V_0\theta}{d_c}\right)\right)\right)\right) - k''\dot{V} - \frac{B}{\theta}\left(1 - \frac{\theta V}{d_c}\right)\right) \end{aligned} \tag{A5}$$

The ballpark values are:

- ✓ Elastic modulus $E = 5 \times 10^{10}\, Pa$
- ✓ Critical fault length $l = 3 \times 10^{-2}\, m$
- ✓ Normal stress $\sigma = 200 \times 10^{6} Pa$
- ✓ Radiation damping coefficient $\eta = 20 \times 10^{6} Pa/(m/s)$
- ✓ $A = 0.011$
- ✓ $B = 0.014$
- ✓ $V_0 = 1 \mu m/s$
- ✓ $\theta_0 = 0.6$
- ✓ $\mu_0 = \mu_0 = 0.6$
- ✓ $t_{start} = 0$, $t_{end} = 50\, s$, $dt = 0.05\, s$

from which the effective stiffness and damping are obtained as

- ✓ $k' = \frac{E}{l\sigma} = \frac{5\times10^{10}}{3\times10^{-2}\times2\times10^{8}}[1/m] \approx 10^{-2}[1/\mu m]$
- ✓ $k'' = \frac{\eta}{\sigma} = \frac{2\times10^{7}}{2\times10^{8}}[s/m] = 10^{-7}[s/\mu m]$

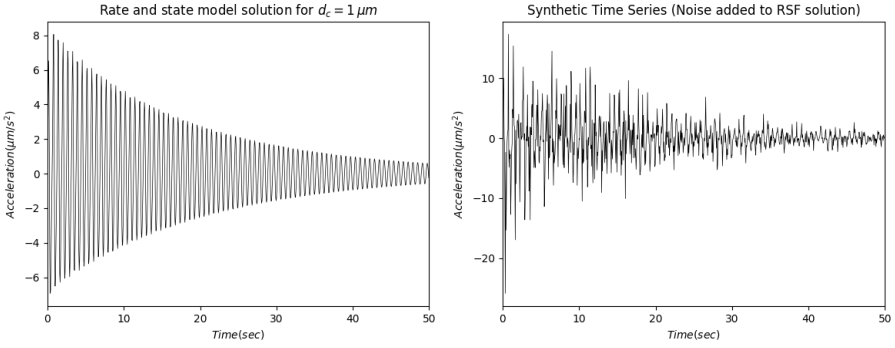

Fig. A2: System response

The influence of critical slip distance on system response to a load point perturbation of the form

$$V_l = V_0(1 + \exp(-t/20)\, sin(10t)) \tag{A6}$$

is shown in Fig. A2.

References

[1] Sak, H., Senior, A., Beaufays, F.: Long short-term memory based recurrent neural network architectures for large vocabulary speech recognition. arXiv preprint arXiv:1402.1128 (2014)

[2] Dana, S., Reddy, K.: Bayesian inference and markov chain monte carlo based estimation of a geoscience model parameter. arXiv preprint arXiv:2201.01868 (2021)

[3] Dana, S., Lyathakula, K.R.: Uncertainty quantification in friction model for earthquakes using bayesian inference. arXiv preprint arXiv:2104.11156 (2021)

[4] Dana, S., Wheeler, M.F.: Convergence analysis of fixed stress split iterative scheme for anisotropic poroelasticity with tensor biot parameter. Computational Geosciences **22**(5), 1219–1230 (2018)

[5] Dana, S., Wheeler, M.F.: Convergence analysis of two-grid fixed stress split iterative scheme for coupled flow and deformation in heterogeneous poroelastic media. Computer Methods in Applied Mechanics and Engineering **341**, 788–806 (2018)

[6] Dana, S., Ganis, B., Wheeler, M.F.: A multiscale fixed stress split iterative scheme for coupled flow and poromechanics in deep subsurface reservoirs. Journal of Computational Physics **352**, 1–22 (2018)

[7] Dana, S., Srinivasan, S., Karra, S., Makedonska, N., Hyman, J.D., O'Malley, D., Viswanathan, H., Srinivasan, G.: Towards real-time forecasting of natural gas production by harnessing graph theory for stochastic discrete fracture networks. Journal of Petroleum Science and Engineering **195**, 107791 (2020)

[8] Dana, S., Jammoul, M., Wheeler, M.F.: Performance studies of the fixed stress split algorithm for immiscible two-phase flow coupled with linear poromechanics. Computational Geosciences, 1–15 (2021)

[9] Dana, S., Ita, J., Wheeler, M.F.: The correspondence between voigt and reuss bounds and the decoupling constraint in a two-grid staggered

algorithm for consolidation in heterogeneous porous media. Multiscale Modeling & Simulation **18**(1), 221–239 (2020)

[10] Dana, S.: Addressing challenges in modeling of coupled flow and poromechanics in deep subsurface reservoirs. PhD thesis, The University of Texas at Austin (2018)

[11] Ruina, A.L.: Slip instability and state variable friction laws. Geophys. Res. Lett. **88**, 359–370 (1983)

[12] Scholz, C.H.: Mechanics of faulting. Ann. Rev. Earth Planet. Sci. **17**, 309–334 (1989)

[13] Marone, C.: Laboratory-derived friction laws and their application to seismic faulting. Ann. Rev. Earth Planet. Sci. **26**, 643–696 (1998)

[14] Wei, M., Shi, P.: Synchronization of earthquake cycles of adjacent segments on oceanic transform faults revealed by numerical simulation in the framework of rate-and-state friction. Journal of Geophysical Research: Solid Earth **126**(1), 2020–020231 (2021)

[15] Jia, Y., Tang, J., Lu, Y., Lu, Z.: The effect of fluid pressure on frictional stability transition from velocity strengthening to velocity weakening and critical slip distance evolution in shale reservoirs. Geomechanics and Geophysics for Geo-Energy and Geo-Resources **7**(1), 1–13 (2021)

[16] Weiqiang, Z., Allison, K., Dunham, E., Yang, Y.: Fault valving and pore pressure evolution in simulations of earthquake sequences and aseismic slip. Nature communications **11**, 4833 (2020)

[17] Palmer, A.C., Rice, J.R.: The growth of slip surfaces in the progressive failure of over-consolidated clay. Proceedings of the Royal Society of London. A. Mathematical and Physical Sciences **332**(1591), 527–548 (1973)

[18] Rice, J.R., Gu, J.-c.: Earthquake aftereffects and triggered seismic phenomena. Pure and Applied Geophysics **121**(2), 187–219 (1983)

[19] Gu, J.-C., Rice, J.R., Ruina, A.L., Simon, T.T.: Slip motion and stability of a single degree of freedom elastic system with rate and state dependent friction. Journal of the Mechanics and Physics of Solids **32**(3), 167–196 (1984)

[20] Dieterich, J.H.: Earthquake nucleation on faults with rate-and state-dependent strength. Tectonophysics **211**(1-4), 115–134 (1992)

[21] Kanamori, H., Brodsky, E.E.: The physics of earthquakes. Reports on

Progress in Physics **67**(8), 1429 (2004)

[22] McClure, M.W., Horne, R.N.: Investigation of injection-induced seismicity using a coupled fluid flow and rate/state friction model. Geophysics **76**(6), 181–198 (2011)